

LA-UR - 89-3503

Los Alamos National Laboratory is operated by the University of California for the United States Department of Energy under contract W-7400-ENG-36

TITLE: PRELIMINARY INTEGRATED CALCULATION OF RADIONUCLIDE CATION AND ANION TRANSPORT AT YUCCA MOUNTAIN USING A GEOCHEMICAL MODEL

AUTHORS:

Lay H. Birkhoff, KES-5
Katherine Campbell, A-1
Kenneth G. Eggert, KES-5
Bryan J. Travis, KES-5

SUBMITTED TO:

Focus '89 Nuclear Waste Isolation in the Unsaturated Zone
Bally's Casino Resort, Las Vegas, NV, September 18-21, 1989

By acceptance of this article, the publisher recognizes that the U.S. Government retains a nonexclusive, royalty-free license to publish or reproduce the published form of this contribution, or to allow others to do so, for U.S. Government purposes.

The Los Alamos National Laboratory requests that the publisher identify this article as work performed under the auspices of the U.S. Department of Energy.

LOS ALAMOS Los Alamos National Laboratory
Los Alamos, New Mexico 87545

FORM NO. 625 1A
BY THE AUTHOR
9307090248 930617
PDR WASTE PDR
WM-11

W00000

LA-UR-89-3503

6 0 0 0 2 0 9 0

Preliminary Integrated Calculation of Radionuclide Cation and Anion Transport at Yucca Mountain Using a Geochemical Model

Kay H. Birdsell, Katherine Campbell, Kenneth G. Eggert,
and Bryan J. Travis

ABSTRACT

36020010

This paper presents preliminary transport calculations for radionuclide movement at Yucca Mountain using preliminary data for mineral distributions, retardation parameter distributions, and hypothetical recharge scenarios. These calculations are not performance assessments, but are used to study the effectiveness of the geochemical barriers at the site at a mechanistic level. The preliminary calculations presented have many shortcomings and should be viewed only as a demonstration of the modeling methodology. The simulations were run with TRACRN, a finite-difference porous flow and radionuclide transport code developed for the Yucca Mountain Project. Approximately 30,000 finite-difference nodes are used to represent the unsaturated and saturated zones underlying the repository in three dimensions. Sorption ratios for the radionuclides modeled are assumed to be functions of mineralogic assemblages of the underlying rock. These transport calculations present a representative radionuclide cation, ^{137}Cs , and anion, ^{99}Tc . The effects on transport of many of the processes thought to be active at Yucca Mountain may be examined using this approach. The model provides a method for examining the integration of flow scenarios, transport, and retardation processes as currently understood for the site. It will also form the basis for estimates of the sensitivity of transport calculations to retardation processes. In part, this model and its quality assured derivatives, will be used to guide the geochemical characterization program.

INTRODUCTION

One of the tasks of the geochemistry program for the Yucca Mountain Project is to provide a geochemical retardation model for the site to those charged with performance assessment calculations. Therefore, a goal of the geochemical characterization program is to understand the effect of site geochemistry on far-field transport calculations from the repository to the accessible environment. We also wish to understand the sensitivity of these calculations to assumptions regarding sorption processes, transport properties, and site mineralogy. One method selected for this task is to formulate a transport model for the site, and use that model to integrate results from mineralogy/petrology work, sorption studies, radionuclide solubility studies, and groundwater chemistry studies. This model will also allow estimation of the changes in retardation that may occur due to changes in

scenarios assumed by performance assessment. This paper reports on the formulation of this model. It also presents preliminary calculations to demonstrate the method. These results should not be viewed as any sort of preliminary performance assessment of the ability of site geochemistry to retard radionuclide transport.

The calculations described in this paper are preliminary, repository-scale, three-dimensional simulations of radionuclide migration from the repository horizon through the unsaturated zone and into the saturated zone. The simulations were run with the computer code TRACRN¹. A three-dimensional geochemical/geophysical model of the tuffs below the repository horizon at Yucca Mountain was constructed for the calculations. The hydrologic component of the model is based on the 3-D hydrological reference stratigraphy developed at Sandia National Laboratory³ from the Topopah Spring welded unit (TSw2) down to the Bullfrog welded unit (BFw). Dipping beds which are offset along the Ghost Dance Fault and a nonhorizontal water table are included. Composite characteristic curves developed by Klavetter and Peters^{2,4} describe the hydrologic properties of the units. The geochemical model includes sorption coefficients that are functions of local mineral assemblage.

Base case calculations for various steady recharge rates (0.1 mm/yr, 0.5 mm/yr, and 4.5 mm/yr), and two radionuclides (⁹⁹Tc and ¹³⁵Cs) are presented, and the effect of dispersivity length scale is examined. The calculations were meant to provide estimates of the effectiveness of the site's geochemical barriers. However, many shortcomings became apparent during the simulations so that they should be viewed only as examples of the modeling methodology. Further calculations using this same modeling approach will form the basis for a subsequent retardation sensitivity analysis for the purpose of guiding the geochemical characterization of the Yucca Mountain site. The calculations will focus in on a smaller 3-D zone under the proposed repository site and study the variations in radionuclide migration rates due to the spatial distribution of sorption coefficients.

CONCEPTUAL MODEL

The conceptual model used for these simulations is made up of four main components: a mathematical model, a hydrologic model, a geochemical model, and a mineralogic/petrologic (min/pet) model. These models are intimately related because, for example, the mathematical model describes the equations of flow and transport for the hydrologic and geochemical models, and the sorption coefficients used in the geochemical model are derived from the mineral distribution developed in the min/pet model.

Mathematical Model - The simulations were run with the computer code TRACRN¹. A subset of the equations embodied within TRACRN form the mathematical model describing flow and transport through the Yucca Mountain tuffs. These equations include conservation of mass for the liquid phase,

$$\partial_t(\epsilon\sigma\rho) + \nabla \cdot (\rho\bar{u}) = \epsilon S \quad (1)$$

conservation of momentum for the liquid phase (Darcy's Law),

$$\bar{u} = \frac{-k}{\mu}(\nabla p + \rho\hat{g}) \quad (2)$$

and conservation of contaminant,

$$\begin{aligned} \partial_t(\epsilon\sigma\rho C_a) + \nabla \cdot (\rho\bar{u}C_a) &= \nabla \cdot (\epsilon\sigma\tau_e D_{a\rho} \nabla C_a) + \epsilon C_a S \\ &+ \nabla \cdot [\epsilon\sigma\bar{D}_a \nabla(\rho C_a)] - \epsilon\lambda_a \sigma\rho C_a \\ &- \rho\rho_m (Kd(\partial_t C_a + \lambda C_a)) \end{aligned} \quad (3)$$

Equation (3) describes diffusive, dispersive and advective transport of a radioactive contaminant undergoing equilibrium sorption. Solution of these equations is obtained by implicit, integrated finite-difference schemes, although an explicit solution scheme is available for the transport equation. The matrix equations are solved using a preconditioned conjugate gradient method.

Hydrologic Model - The hydrologic model includes the stratigraphy, the hydrologic properties of the units, the imposed recharge rates, and the position of the water table. The stratigraphy is based on the three-dimensional reference stratigraphic model of Yucca Mountain developed by Ortiz, et. al.² The stratigraphic units included in the model are those from the repository horizon down to the Bullfrog welded unit. From top to bottom these units include,

- Topopah Spring welded, lithophysae-poor (TSw2);
- Topopah Spring welded, vitrophyre (TSw3);
- Calico Hills and Lower Paintbrush nonwelded, vitrophyre (CHnv);
- Calico Hills and Lower Paintbrush nonwelded, zeolitized (CHnz);
- Prow Pass welded, (PPw);
- Upper Crater Flat nonwelded, (CFUn); and
- Bullfrog welded (BFw).

The CHnv and CHnz units incorporate the three Calico Hills units (CHn1, CHn2, and CHn3) and are differentiated by the position of the zeolitized zone (TZZ) given by Ortiz et. al.² The position of the water table is also taken from their model. Data from Nevada coordinates 757,000 ft to 772,000 ft north and 557,000 ft to 566,000 ft east is

included in the modeled area. The units dip at about 6° from west to east. The Ghost Dance Fault zone is located at approximately 562,400 ft east and dips from 5° to 10°.

Composite characteristic curves developed by Klavetter and Peters^{3,4,5} were used to describe the hydrologic properties of the units. The curves represent composite-porosity properties i.e., matrix and fracture properties are combined to form a single characteristic curve for each unit. The composite-porosity model is a simplified dual-porosity model that assumes equivalent pressures locally in the matrix and fractures^{3,5}. Figures 1 and 2 show conductivity curves for the TSw2 and PPw units. The double plateaued composite curve (Fig. 1) is a typical curve for a tuff with a high fracture porosity and fracture conductivity. The single plateaued composite curve (Fig. 2) is typical of a sparsely fractured tuff with a high matrix saturated conductivity. Composite properties are available for TSw2, TSw3, CHnv, CHnz, and PPw⁵. Matrix conductivity curves are reported⁶ for the CFUn and BFW units. Composite curves were constructed for these units by using the fracture properties of the CHnz and PPw units respectively, because of the similarity in fracture characteristics between the CFUn unit and the CHnz unit, and between the BFW and the PPw unit.

Recharge rates of 0.1 mm/yr, 0.5 mm/yr, and 4.5 mm/yr were used to establish three steady flow fields through the mountain. These recharge rates are estimates and were chosen to provide scenarios that produce various combinations of matrix and fracture flow. To simulate this recharge a constant flux was applied to the upper boundary, which corresponds to the repository horizon.

Geochemical model - The main constituent of the geochemical model is the spatial distribution of sorption coefficients as a function of mineral assemblage. The min/pet model described below explains the geostatistical analysis of mineral distributions that was subsequently used to construct maps of spatially distributed sorption coefficients. Other important constituents of the geochemical model are the magnitude of the longitudinal and transverse dispersivity length scales, the source terms for the radionuclides as they are released from the repository along with the position and shape of the repository itself, and diffusion coefficients for the radionuclides in the different tuffs.

Simulations of the transport of technetium (Tc^{99}) and cesium (Cs^{135}) for a 20,000 yr period were run. The sorption coefficient (Kd) for Tc depends on the abundance of the minerals hematite and mica,

$$Kd_{Tc} = Kd_{hem}X_{hem} + Kd_{mica}X_{mica} \quad (4)$$

where $Kd_{hem} = 5.3$ ml/g is the sorption coefficient of Tc on pure hematite, $Kd_{mica} = 3.4$ ml/g is the sorption coefficient of Tc on pure mica, and X is the weight fraction of the mineral. Kd for Cs varies with the abundance of clinoptilolite, montmorillonite, mordenite, analcime, and glass in the tuff⁶.

0000000000

$$Kd_{Cs} = Kd_{clin} \sum W_i X_i \quad (5)$$

where $Kd_{clin} = 3.8 \times 10^4$ ml/g is the sorption coefficient for Cs on pure clinoptilolite, and the W_i 's are weighting factors for each mineral. The W_i 's represent the ratio of the mineral's Kd to that of clinoptilolite. They range from 0.50 for montmorillonite to 0.016 for glass. Table 1 shows the minimum, average, and maximum simulated Kd values for Tc and Cs in the seven min/pet layers discussed below.

TABLE 1: Minimum, Average And Maximum Simulated Kd Values For Cesium And Technetium In Seven Layers

| | CESIUM | | | TECHNETIUM | | |
|---------------|--------|--------|--------|------------|-------|-------|
| | Min | Avg | Max | Min | Avg | Max |
| TSw2 (6981) | 0. | 0. | 0. | 0.011 | 0.038 | 0.093 |
| ZI (776) | 1110. | 3751. | 9384. | 0.011 | 0.035 | 0.091 |
| VITRIC (5311) | 374. | 743. | 2011. | 0.002 | 0.023 | 0.090 |
| CHnz (6072) | 490. | 18120. | 37306. | 0.0003 | 0.048 | 0.712 |
| PPw (2455) | 0. | 0. | 0. | 0.004 | 0.018 | 0.073 |
| CFun (6141) | 607. | 12638. | 33884. | 0.000 | 0.000 | 0.000 |
| BFw (2693) | 0. | 0. | 0. | 0.032 | 0.099 | 0.285 |

These species were chosen for the simulations because of their different transport properties. Tc forms the anion TcO_4^- which will not cation exchange with the zeolites or clays in the tuffs. Because the abundance of hematite and mica in the tuffs is low, its sorption coefficient is low. Cs acts as a simple cation. It is thought to undergo cation exchange with the zeolitic tuffs and consequently has a very high sorption coefficient. Sorption coefficients for other radionuclides should be between those of Cs and Tc. Both of these radionuclides have long halfives of order 10^5 to 10^6 years.

The dispersivity length scales are unknown for field-scale transport through the Yucca Mountain tuffs. The simulations were run using different longitudinal and transverse dispersivities to study their effect on radionuclide migration. Longitudinal dispersivities of 10 m and 1 m, and transverse dispersivities of 1 m and 0.1 m were run with ratios of longitudinal to transverse dispersivities of 10:1. The large dispersivity values assumed here result from scaling data from column studies up to repository scale.

Release rates from the repository vary with time. Estimates of these release rates were not available at the time these simulations were run. A steady source of $C_0 = 1$ released at the recharge rate was used to calculate relative concentrations since the source term is unknown. The release area roughly follows the proposed shape and position of the repository⁷. Release is homogeneous from the repository (i.e., panels of canisters or individual canisters are not considered). With this source term, actual quantities of radionuclides

36020014

00000000

released to the accessible environment can not be estimated, but the effectiveness of the site's geochemical barriers can be investigated and some sensitivity analysis calculations can be performed.

The same diffusion coefficient was used for the two radionuclides in the various tuffs. Typical aqueous diffusion coefficients are on the order of 10^{-8} cm²/s. Diffusion experiments in saturated cores show that the tortuosity decreases the effective diffusion coefficient by a factor of approximately 0.05 in the Topopah Spring core samples and by 0.07 in the Calico Hills samples⁸. The effective diffusion coefficient also decreases with saturation, but this dependence is not yet known for the Yucca Mountain tuffs. Tortuosity values of 0.05 and diffusion coefficients of 10^{-8} cm²/s were used.

36020015
Mineralogic/Petrologic Model - For the purposes of simulating mineral distributions, the block was divided into seven units. Five of these are the same as the hydrologic units listed above: TSw2, CHus, PPw, CFUn and BFW. The sixth combines the vitric units TSw3 and CHv, except for a thin smectite-bearing scolded layer at the top of the basal vitrophyre of the Topopah Spring member⁹ that is treated as a separate, seventh unit.

Except for this seventh unit, these layers are represented by 17 to 75 observations each in a data base containing x-ray diffraction measurements for samples from twelve drill holes near the target development area. Alkali-feldspar and the silica polymorphs quartz, tridymite and cristobalite are widely observed, and glass, clinoptilolite, mordenite, smectite, mica, calcite and hematite also occur in measurable quantities in some or all of these units.

Geostatistical simulation of the spatial distribution of these minerals throughout the block is based on spatial covariance models for the logarithmic ratios $r = \log(m/a)$, where m is the abundance of a given mineral and a is the abundance of the ubiquitous mineral alkali-feldspar.¹⁰ The parameters of these covariance models were estimated from these data, although in many cases the data are too sparse to form reliable estimates. These models and the individual observations were used to construct conditional simulations¹¹ of average mineral composition within each of the more than 30,000 blocks defining the finite difference zones used in TRACRN (see below). These average mineral compositions were then converted to average sorption coefficients for each block using the geochemical model described above. The distributions of sorption coefficients thus obtained are summarized by unit in Table 1.

SIMULATIONS

Grid - The bedded tuffs dip at approximately 6° from west to east. The stratigraphic data was rotated upward 6° and translated to facilitate gridding of the units. The data was also converted to meters to match input requirements for TRACRN. A nonvertical gravity vector compensates for the rotation of the beds. The grid is made up of 30,870

finite difference zones. This quantity was chosen because it is near the maximum problem size that can be run with TRACRN using the memory allocated per user on the Cray Y-MP's at Los Alamos National Laboratory (about 4.2 million words out of 5.0 million words allowed). There are 15 300-m blocks in the north-south direction, 37 73-m blocks in the east-west direction with 5 finer blocks near the Ghost Dance Fault zone, and 49 blocks from an elevation of 50 m to 450 m. The Ghost Dance Fault zone is located at 1695 m East and is 5 m wide. The vertical zones range in thickness from 2 m to 18 m. The beds vary in thickness and in elevation throughout the modeled region. The grid captures much of this variation. Offset along the fault zone is included in the material layer set-up, although the fault zone is not explicitly modeled as a different material (i.e., it has the material properties of the adjacent unit).

3 6 0 2 0 0 1 6

Source Terms - The recharge rate was treated as a source term for the simulations. Each of the finite difference blocks at the upper boundary supplied water at the appropriate recharge rate. The radionuclide source term was treated similarly, except that only finite difference cells within the boundary of the repository block supplied radionuclide at a concentration of 1.0 g/g fluid. The release area has roughly the same shape and position as that planned for the potential repository block². The leachate rate was considered to be the same as the recharge rate. The flow field was brought to steady state for the three flow rates. The transport simulations were then run under steady flow conditions.

Hydrologic Properties - Characteristic curves of capillary pressure and relative permeability as functions of saturation were constructed for each hydrologic unit based on the composite properties discussed previously. The curves are highly nonlinear as the fractures saturate, which generally occurs at composite saturations greater than 0.999. Because both the saturated and the unsaturated zones are considered in these simulations, calculational difficulties occurred in finite difference zones adjacent to the water table due to the extreme nonlinearity of these curves. For these preliminary calculations, the curves were consequently linearized from composite saturations of 0.99 to 0.9999 for units TSw2 and TSw3 and from 0.99 to 0.99999 in units CFUn and CHnz to help the simulations converge more rapidly. The effect of this linearization is that the fractures saturate over a larger saturation range. This causes the relative permeability to increase more gradually although the increase begins at a lower composite saturation value.

Water Table - The water table at Yucca Mountain rises sharply to the northwest. It was included in these calculations because the distance from the repository to the water table varies significantly with position. A planar surface was initially defined based on data points from the water table surface included in the stratigraphic model² used for these simulations. Constant pressure boundary conditions hold the water table at its initial level at the boundaries. It fluctuates some with recharge rate, but is artificially held close to its initial position by the imposed pressures at the bottom and side boundaries. Because the stratigraphic data was rotated upward along the dipping beds, the simulated water table was also rotated and appears to be far from horizontal in the results that follow.

00000000

3
6
0
2
0
0
1
7

Flow Results - Figures 3 through 5 show pressure, saturation, and velocity plots at the 0.5 mm/yr flow rate through an East-West cross section of the mountain. The stratigraphy used for the calculations is superimposed on the pressure plots to show its strong influence on the flow and transport solutions. The simulated water table is nonhorizontal because it is rotated to offset the rotation of the stratigraphic data, and also because it mimics the northwesterly rise observed at the mountain. Plots for the 0.1 mm/yr and the 4.5 mm/yr recharge rates look very similar to these plots. It may be because the position of the water tables does not vary with flow rate because it is over constrained. In the velocity vector plot, strong lateral flow can be identified in the CHv and PPw units, and the finer gridding along the fault zone at 1695 m East is evident. Although the fault has no explicit properties of its own, the offset of beds along the fault is causing some of the lateral flow along bedding planes to be diverted downward. Figure 6 shows saturation profiles through a North-South cross section of the mountain. By comparing Figures 4 and 6, the 3-dimensionality of the flow field becomes apparent. The flow solutions were assumed to be at steady state when the flow solution converged rapidly and pressure and saturation results at progressively larger times compared well. This may or may not have been adequate considering that the small pressure and saturation changes that occur near full saturation can cause drastic changes in velocity. Nevertheless, the "steady" flow solutions were used for subsequent transport calculations.

Transport Results - Figures 7 through 9 show log-scale fluid concentration plots for ^{99}Tc at 20,000 yr at a 0.1 mm/yr recharge rate for the two cross sections shown above. The positions of the water table and the repository are also given for each cross section. The East-West section shown is a section where the species migrate at a moderate rate. The North-South cross section (Fig. 9) presented represents a section where migration toward the water table is fastest. Two sets of dispersivity length scales are presented for the calculations shown. For Fig. 7, a longitudinal dispersivity of 10 m (used in the vertical direction) with a transverse dispersivity (used in the horizontal direction) of 1 m was used. For Figs. 8 and 9, a longitudinal value of 1 m and a transverse value of 0.1 m were used. At this flow rate, the assumed dispersivity strongly affects the transport solution. For the East-West cross section shown, technetium concentrations as high as $10^{-6} C_0$ for the high dispersivity case (Fig. 7), and $10^{-8} C_0$ for the lower dispersivity case (Fig. 8) intercept the water table. A factor of 10 difference in the dispersivity length scale resulted in a factor of 100 difference in the concentration breaking through to the water table for this particular cross section. Vertical flow occurring along the fault zone is evident in these plots at 1695 m East by the downward dip in the concentration plumes at that position. Figure 9 shows ^{99}Tc concentrations as high as $10^{-3} C_0$ reaching the water table in the region of fastest flow. This shows that the solution to the transport problem at Yucca Mountain is also three-dimensional. Figure 10 presents a log-scale solid concentration plot for ^{99}Tc that has sorbed onto the tuffs. This figure corresponds to the fluid concentration plot shown in Fig. 8. The solid concentration in unit CFU is zero because that unit was assumed to be nonsorbing for technetium.

Figures 11 and 12 show log-scale fluid concentration profiles at the 0.5 mm/yr recharge rate for the East-West cross section. Concentration profiles for the two dis-

persivity length scales are presented. Slightly larger concentrations are shown for the 0.5 mm/yr cases (Figs. 11 and 12) than for the 0.1 mm/yr cases (Figs. 7 and 8), although the results are very similar.

At the high recharge rate (4.5 mm/yr), initial calculations showed high concentrations breaking through to the water table, but the solutions seemed to be very disperse. These calculations, and the ones presented above, were run using the implicit finite difference solution for the transport equation available in TRACRN. The solution is stable for any time step, although numerical dispersion increases as the time step increases. TRACRN also has an option to solve the transport equation explicitly. The time step is controlled by the courant limit, and numerical dispersion is further controlled with a correction term. We can also solve the transport equation using particle tracking which is inherently much less diffusive. A few calculations were run to compare the implicit and explicit solutions. Figures 13 and 14 show concentration profiles at 5,000 yr for ^{99}Tc at the 4.5 mm/yr recharge rate using the two techniques. The explicit technique (Fig. 14) shows less dispersion than the implicit technique (Fig. 13). The plume does not migrate as rapidly toward the water table, and it has more structure than the plume generated using the implicit solution. These results show that numerical dispersion may be causing technetium to break through to the water table too rapidly. These calculations were not pursued further for this study because the explicit runs take considerably more computer time.

Figures 15 and 16 show log-scale fluid concentration plots for ^{137}Cs for the two cross sections at the fastest flow rate. Figure 17 shows a log-scale solid concentration plot corresponding to Figure 15. Results using the high dispersivity length scale are presented here so that these plots show the most rapid migration of cesium of any of the calculations run. The figures show that cesium's high sorptivity successfully retards its migration.

RECOMMENDATIONS

Work on integrating the results of retardation, mineralogic and petrologic studies with transport calculations to develop a geochemical/geophysical model of Yucca Mountain is only beginning. This paper provides an indication of the starting point for work with this model. A number of studies will be required before we can view the results of these calculations as providing an understanding of the effectiveness of geochemical retardation barriers. This understanding will require improvements in all four parts of the conceptual model described above. Recommendations for improvements to the model are given below. These improvements are necessary to enhance confidence in the results of our transport calculations.

Mathematical and Numerical Model - Specifically, with regard to the TRACRN code, numerical dispersion and grid orientation effects will be studied. Higher resolution simulations will be performed, both on the repository as a whole, and on portions of the repository. As needed, new sorption models and a method of utilizing the results of

86020018

ms04/70

groundwater chemistry studies will be incorporated into the code. Particle tracking will be tried as an alternative method for solving transport. Although partially verified, the code is currently undergoing additional verification studies for quality assurance purposes. Several validation exercises are planned. The code will be used to design experiments and provide estimates of experimental results. Finally, three-dimensional runs are expensive, even with an efficient code such as TRACRN. Work will continue to expand the size of the problem that can be addressed, and to improve computational speed.

Hydrologic Model - Site characterization studies will provide a better understanding of the site conceptual hydrologic model, as well as improve estimates of hydrologic parameters. The composite-porosity method, as implemented for these simulations, is inadequate for transport calculations when fracture flow exists. The method smears out fracture velocities by combining them with matrix velocities. This may underestimate advective transport along fractures and overestimate matrix diffusion. Modeling studies are being done to determine the effect that the individual components of matrix and fracture flow have on radionuclide migration under different recharge scenarios. Results of these studies will be incorporated into the model. Further, the Ghost Dance Fault zone will be modeled explicitly, and the water table will be less constrained. More realistic recharge scenarios will also be included as they become available.

Geochemical and Mineralogic/Petrologic Model - Geochemical studies during site characterization are expected to provide refinement in geochemical retardation process assumptions and in their relation to the mineralogic/petrologic models. The current simulations use only one realization of mineral distribution. Many more are required to obtain statistically realistic results.

Studies will be conducted to better understand the dispersion process. Dispersivity length scales may need to be coupled to recharge scenarios. Saturation effects can strongly effect dispersivities, especially when flow patterns change from matrix- to fracture-dominated flow.

A more realistic source term is essential in evaluating the effectiveness of the site's geochemical barriers and in predicting quantities of radionuclides that may reach the accessible environment. These calculations assume a constant source leaching at the recharge rate over the full 20,000 yr period. Actual leachate rates will vary with time and recharge rate and depend on the inventory and the solubility of the particular radionuclide. Limited inventories may result in depleted source terms for some species long before the 20,000 yr period used for these calculations.

CONCLUSIONS

This paper describes our first attempt at modeling transport at Yucca Mountain using spatially distributed stratigraphic, geochemical, and mineralogic data in three dimensions. Work will continue to improve this model based on the recommendations given

above and as further information from site characterization becomes available. The calculations demonstrate that migration from the potential repository is three dimensional, especially for less sorptive species. Some studies will need to treat it as such. For weakly sorbing species like technetium, more studies are required to understand factors controlling transport properties and factors relating to predicting its migration.

8 6 0 2 0 0 2 0

REFERENCES

1. B. J. TRAVIS and K. H. BIRDSELL, "TRACRN 1.0: A Model of Flow and Transport in Porous Media for the Yucca Mountain Project," *LA-UR-88-3986*, Los Alamos National Laboratory (1988).
2. T. S. ORTIZ, R. L. WILLIAMS, F. B. NIMICK, B. C. WHITTET, and D. L. SOUTH, "A Three-Dimensional Model of Reference Thermal/Mechanical and Hydrological Stratigraphy at Yucca Mountain, Southern Nevada," SAND84-1076, Sandia National Laboratories (1985).
3. R. R. PETERS and E. A. KLAVETTER, "A Continuum Model for Water Movement in an Unsaturated Fractured Rock Mass," *Water Resources Research*, 24, 3 (1988).
4. R. R. PETERS, E. A. KLAVETTER, I. J. HALL, S. C. BLAIR, P. R. HELLER, and G. W. GEE, "Fracture and Matrix Hydrologic Characteristics of Tuffaceous Materials from Yucca Mountain, Nye County, Nevada," SAND84-1471, Sandia National Laboratories (1984).
5. A. L. DUDLEY, R. R. PETERS, J. H. GAUTHIER, M. L. WILSON, M. S. TIERNEY, and E. A. KLAVETTER, "Total System Performance Assessment Code (TOSPAC) Volume 1: Physical and Mathematical Bases," SAND85-0002, Sandia National Laboratories (1988).—
6. W. R. DANIELS, et.al., "Summary Report on the Geochemistry of Yucca Mountain and Environs," *LA-9328-MS*, Los Alamos National Laboratory (1982).
7. H. R. MACDOUGALL, L. W. SCULLY, and J. R. TILLERSON, "Site Characterization Plan Conceptual Design Report," SAND84-2641, 6, drawing R07003A, Sandia National Laboratories (1987).
8. R. S. RUNDBERG, I. PARTOM, M. A. OTT, A. J. MITCHEL, and K. BIRDSELL, "Diffusion of Nonsorbing Tracers in Yucca Mountain Tuff," *YMP Milestone R524*, Los Alamos National Laboratory (1987).
9. D. L. BISH and D. T. VANIMAN, "Mineralogical Summary of Yucca Mountain, Nevada," *LA-10532-MS*, Los Alamos National Laboratory (1985).
10. J. AITCHISON, *The Statistical Analysis of Compositional Data*, Chapman and Hall, London (1986).
11. A. G. JOURNAL and Ch. J. HUIJBREGTS, *Mining Geostatistics*, Academic Press, London (1978).

86020022

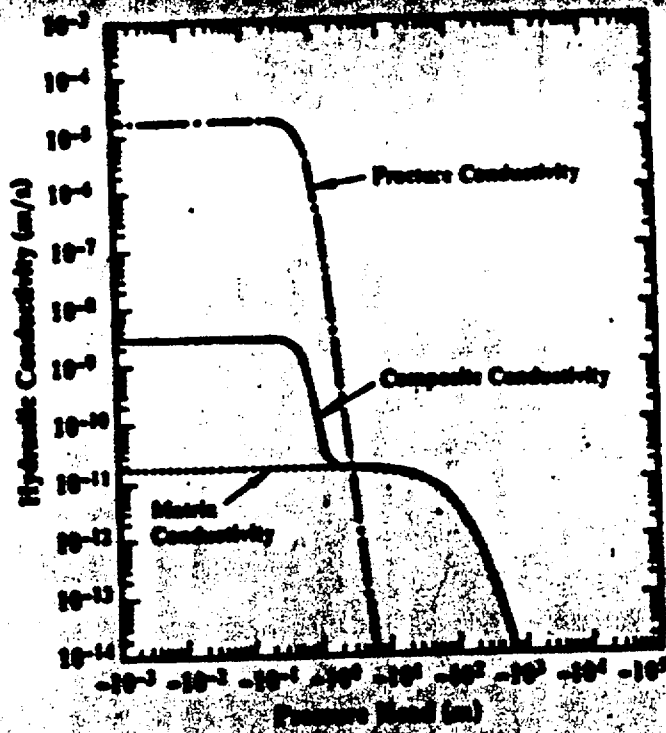


FIGURE 1. CONDUCTIVITY CURVE FOR TSw2.

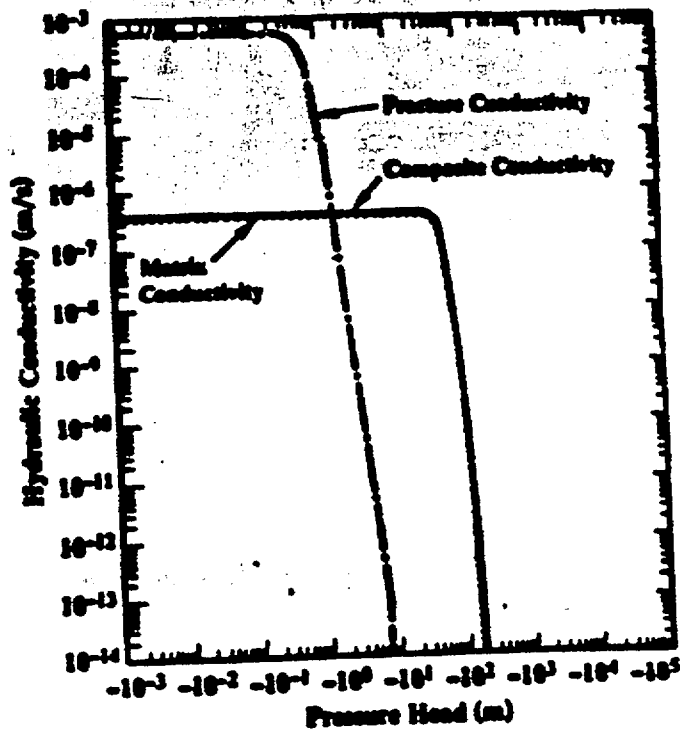


FIGURE 2. CONDUCTIVITY CURVE FOR PTn.

8 6 0 2 0 0 2 3

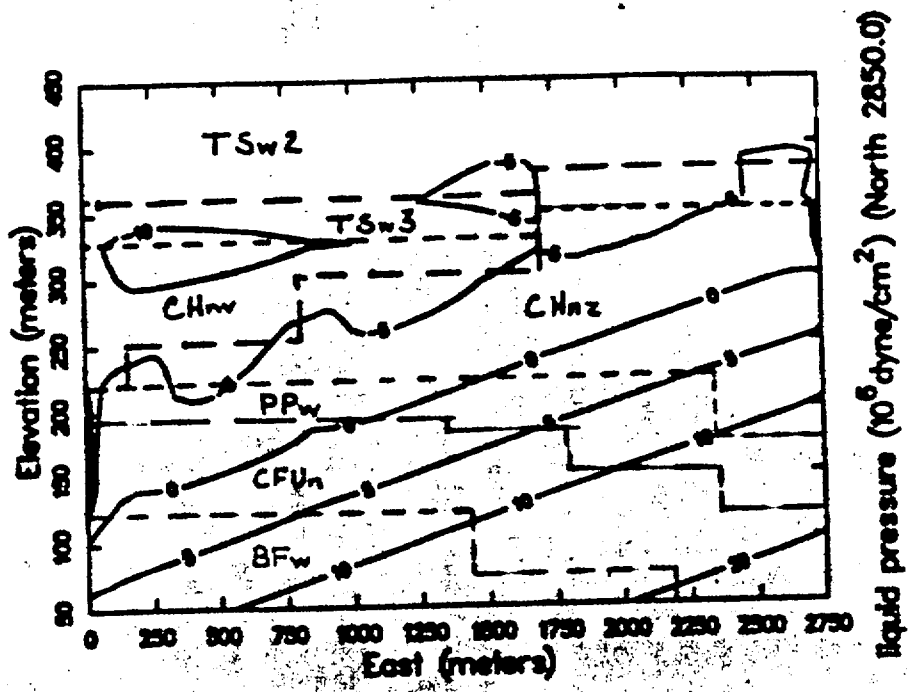


FIGURE 3. LIQUID PRESSURE CONTOURS (10^6 DYNES/CM²) AT A CONSTANT RECHARGE OF 0.5 MM/YR.

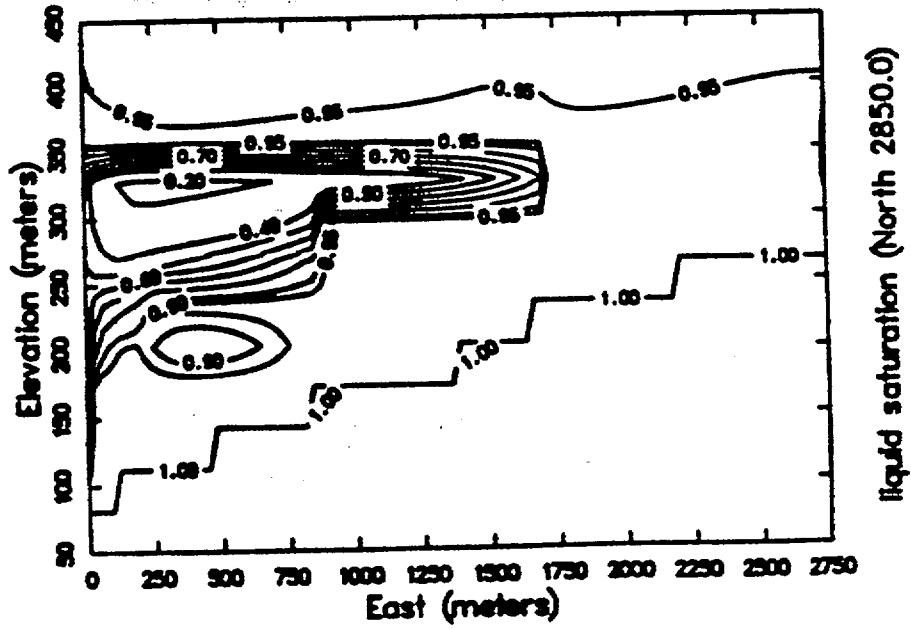


FIGURE 4. SATURATION CONTOURS AT A CONSTANT RECHARGE OF 0.5 MM/YR.

3 6 0 2 0 0 2 4

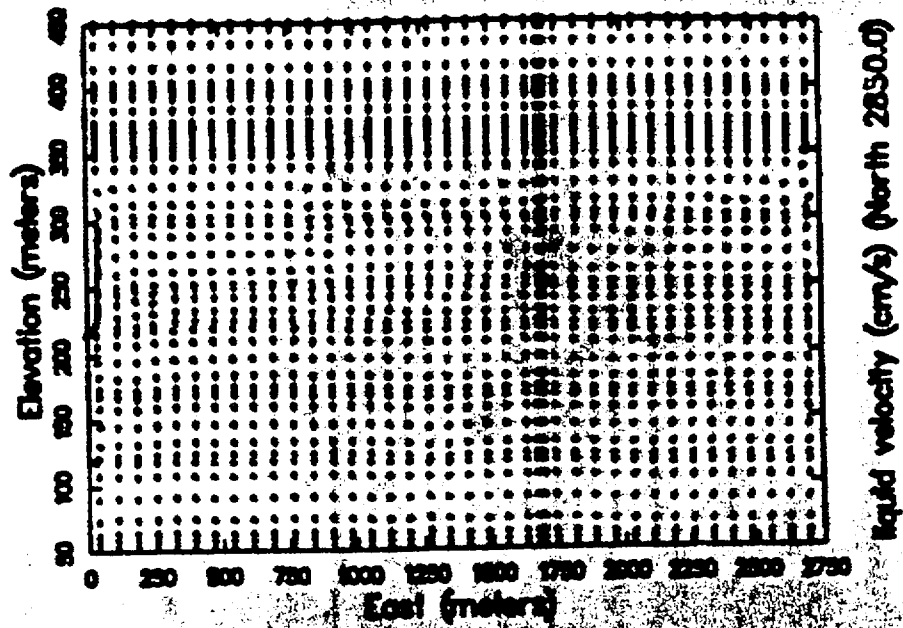


FIGURE 5. VELOCITY VECTORS AT A CONSTANT RECHARGE OF 0.5 MM/YR.

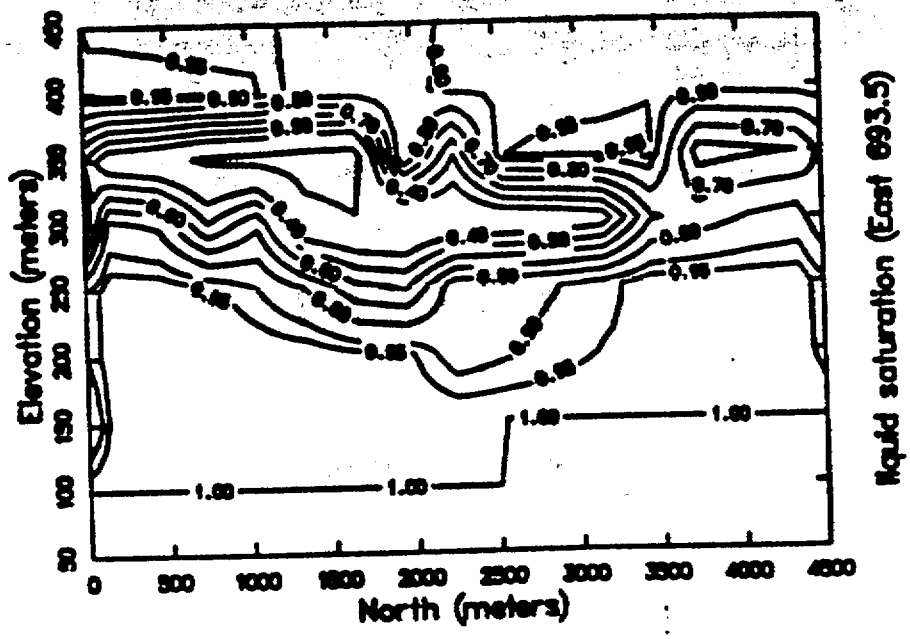


FIGURE 6. SATURATION CONTOURS AT A CONSTANT RECHARGE OF 0.5 MM/YR.

8 6 0 2 0 0 2 5

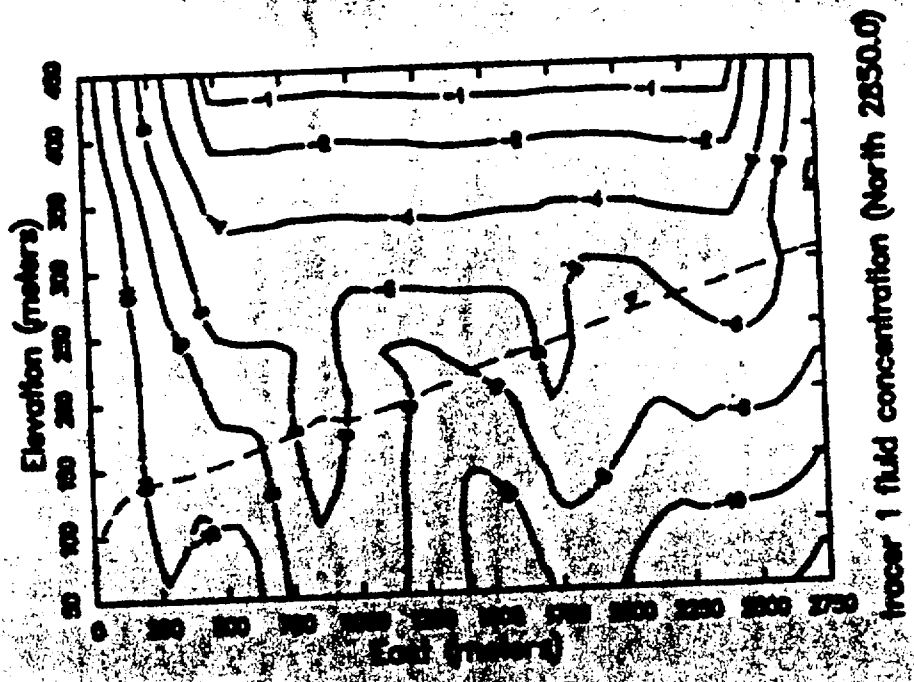


FIGURE 7. LOG-SCALE CONCENTRATION PROFILES FOR ^{99}Tc ALONG A MODERATE MIGRATION PATH AT 20,000 YRS, RECHARGE = 0.1 MM/YR, DISPERSIVITY = 10M, 1M.

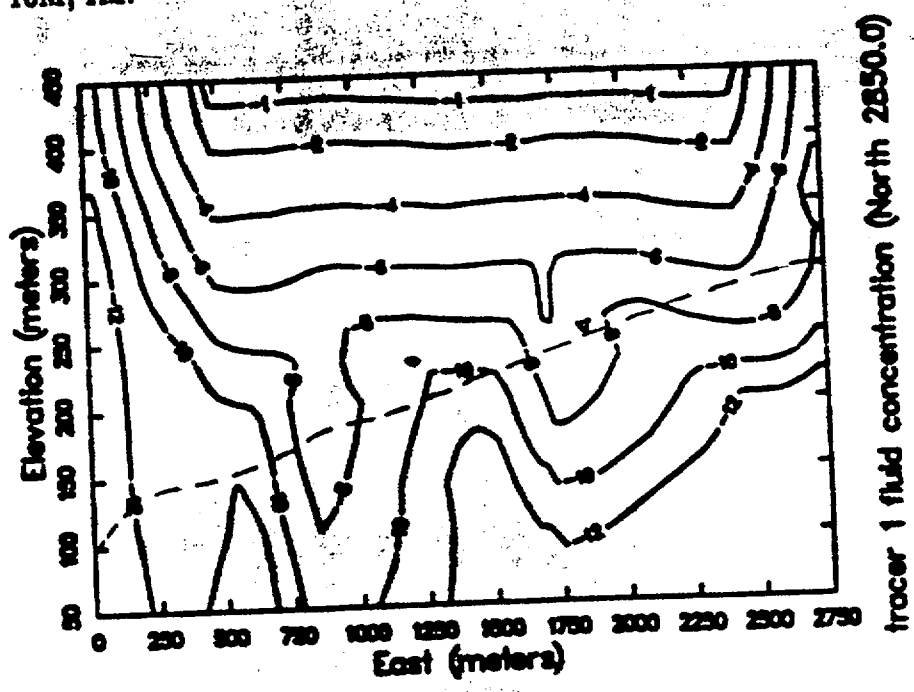


FIGURE 8. LOG-SCALE CONCENTRATION PROFILES FOR ^{99}Tc ALONG A MODERATE MIGRATION PATH AT 20,000 YRS, RECHARGE = 0.1 MM/YR, DISPERSIVITY = 1M, 0.1M.

8 6 0 2 0 0 2 6

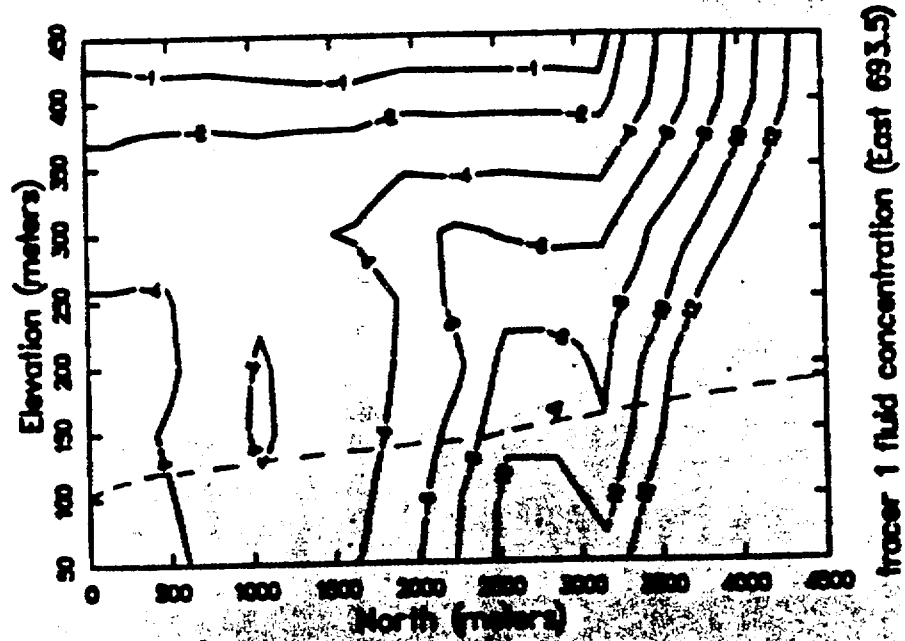


FIGURE 9. LOG-SCALE CONCENTRATION PROFILES FOR ^{99}Tc ALONG A FAST MIGRATION PATH AT 20,000 YRS, RECHARGE = 0.1 MM/YR, DISPERSIVITY = 1M, 0.1M.

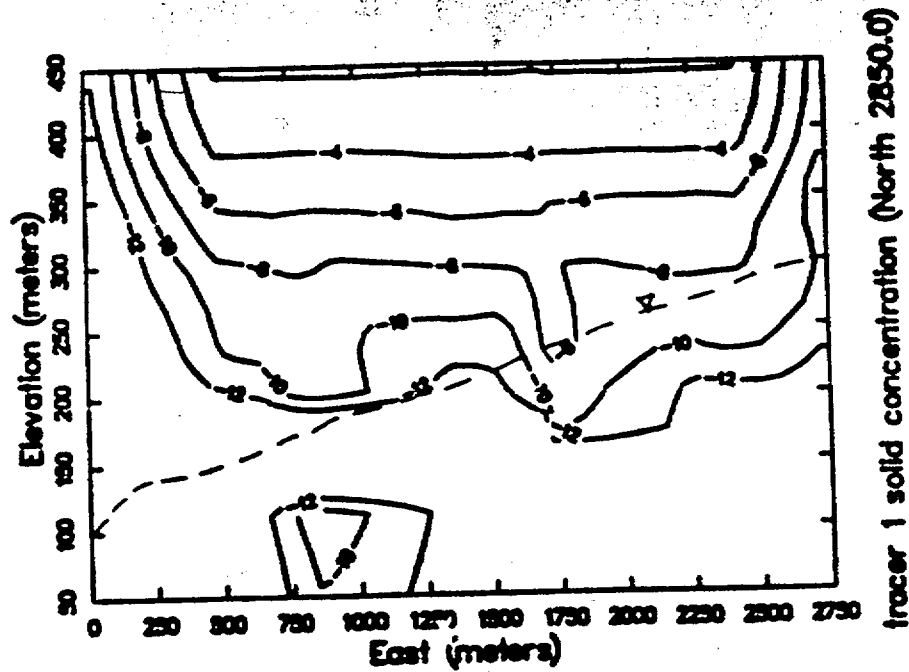


FIGURE 10. LOG-SCALE SOLID CONCENTRATION PROFILES FOR ^{99}Tc ALONG A MODERATE MIGRATION PATH AT 20,000 YRS, RECHARGE = 0.1 MM/YR, DISPERSIVITY = 1M, 0.1M. CORRESPONDS TO LIQUID CONCENTRATION PLOT, FIG. 8.